Journal of Hydrology 587 (2020) 124980

Contents lists available at ScienceDirect

Journal of Hydrology

journal homepage: www.elsevier.com/locate/jhydrol

Research papers

Evaluation of two generalized complementary functions for annual evaporation estimation on the Loess Plateau, China

Haixiang Zhou[a,d], Songjun Han[c], Wenzhao Liu[b,*]

[a] State Key Laboratory of Soil Erosion and Dryland Farming on the Loess Plateau, Institute of Soil and Water Conservation, CAS & MWR, Yangling, Shaanxi 712100, China
[b] Institute of Soil and Water Conservation, Northwest A&F University, Yangling, Shaanxi 712100, China
[c] State Key Laboratory of Simulation and Regulation of Water Cycle in River Basin, China Institute of Water Resources and Hydropower Research, Beijing 100038, China
[d] University of the Chinese Academy of Sciences, Beijing 100049, China

ARTICLE INFO

This manuscript was handled by Marco Borga, Editor-in-Chief

Keywords:
Annual evaporation
Complementary principle
Generalized nonlinear advection aridity model
Sigmoid generalized complementary function
Loess Plateau

ABSTRACT

Generalized complementary functions, which describe the relationship between the ratio of actual evaporation over the Penman potential evaporation (E/E_{Pen}) and the proportion of the radiation term in E_{Pen} (E_{rad}/E_{Pen}) have not been widely used at annual time scales. In this study, the generalized nonlinear advection-aridity function (GNAA) and sigmoid generalized complementary function (SGCF) were evaluated for annual evaporation estimation with calibrated parameters in the Loess Plateau of China. For all 15 catchments, the lowest values of annual E_{rad}/E_{Pen} were found to be much larger than zero, and the annual E/E_{Pen} increased approximately linearly with annual E_{rad}/E_{Pen}. This complementary evaporation relationship at an annual timescale differs from those at daily timescales, and requires different parameterizations of the GNAA and SGCF. For the GNAA, parameter c, which is often set to zero for daily time scales, need to be well calibrated with available data. For the SGCF, the upper and lower limits of E_{rad}/E_{Pen} must be constrained. After calibration, both the SGCF and GNAA performed well at estimating annual evaporation. In addition, the calibrated Priestley-Taylor coefficient from the SGCF was found to be closer to the widely accepted value (1.26) than that determined from the GNAA.

1. Introduction

The complementary principle provides the basis for approaches to estimate actual evaporation by using routine meteorological records only (Brutsaert and Stricker, 1979; Han et al., 2012; Morton, 1983). It has attracted significant attention in recent years, as it can be implemented without the need of explicit land, soil, and vegetation information (Brutsaert, 2015; Han and Tian, 2018). The original complementary principle involves a linear complementary relationship (CR) between actual evaporation (E), potential evaporation (E_{po}), and apparent potential evaporation (E_{pa}), in which E and E_{pa} depart from E_{po} in opposite directions when the land surface is drying from completely wet conditions with a constant energy input (Brutsaert, 2015). Several evaporation estimation models based on the CR have been proposed after specifying E_{pa} and E_{po} (Brutsaert and Stricker, 1979; Granger, 1989; Granger and Gray, 1989; Morton, 1978, 1983). The advection-aridity (AA) model proposed by Brutsaert and Stricker (1979) is the most widely used. In AA model, E_{pa} and E_{po} are denoted by the Penman equation (E_{Pen}) (Penman, 1948) and the Priestley-Taylor (1972) equation, respectively. The AA model has since evolved to adopt the asymmetric CR (Brutsaert and Parlange, 1998; Szilagyi, 2007). Normalized by E_{Pen}, the AA model can be expressed as a linear function (Han et al., 2008):

$$\frac{E}{E_{Pen}} = \left(1 + \frac{1}{b}\right)\alpha_e \frac{E_{rad}}{E_{Pen}} - \frac{1}{b} \tag{1}$$

where α_e is the Priestley-Taylor coefficient, b is the parameter denoting the asymmetry of the CR, and E_{Pen} is an apparent potential evaporation calculated by the Penman equation:

$$E_{Pen} = E_{rad} + E_{aero} = \frac{\Delta}{\Delta + \gamma}(R_n - G) + \frac{\gamma}{\Delta + \gamma} f(u_z)(e_a^* - e_a) \tag{2}$$

where E_{rad} and E_{aero} are the radiation and aerodynamic terms for the Penman equation, respectively (mm/day); Δ is the slope of the saturation vapor curve at air temperature (hPa/°C); γ is the psychrometric constant (hPa/°C); R_n is net radiation (mm/day); G is the ground heat flux; $f(u_z)$ is the wind function, which is calculated by Penman's wind function (Penman, 1948), that is, $f(u_2) = 0.26(1 + 0.54u_2)$, and $u_2 = u_{10}\,(2/10)^{1/7}$, where u_2 and u_{10} are the wind speeds at 2 m and 10 m heights, respectively; and e_a* and e_a are saturation and actual

* Corresponding author.
E-mail address: wzliu@ms.iswc.ac.cn (W. Liu).

https://doi.org/10.1016/j.jhydrol.2020.124980
Received 30 September 2019; Received in revised form 26 March 2020; Accepted 15 April 2020
Available online 23 April 2020

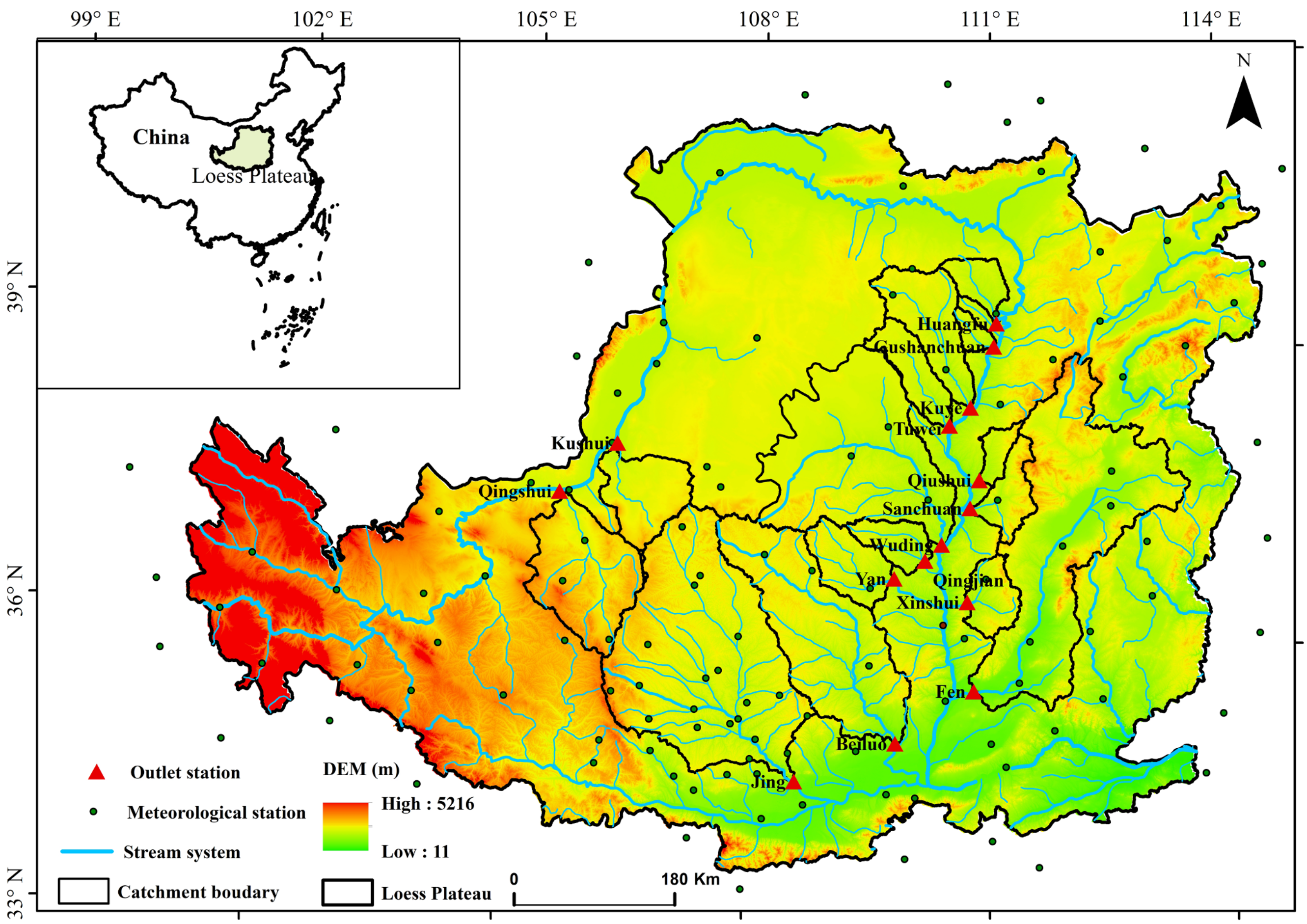

Fig. 1. Locations of the 15 catchments on the Loess Plateau.

vapor pressure (hPa), respectively.

By normalizing several existing CR models using E_{Pen}, Han et al. (2011, 2012) proposed a general form of the CR where the actual evaporation ratio (E/E_{Pen}) is expressed as a function of the proportion of the radiation term in E_{Pen}; that is, $E/E_{Pen} = f(E_{rad}/E_{Pen})$. The AA model is a linear analytical form of this generalized complementary function that has bias under arid and wet environments (Han et al., 2011, 2012). By invoking boundary conditions for extremely arid and completely wet environments, Han et al. (2012) derived a sigmoid form of the generalized complementary function, and updated it by introducing minimum (x_{min}) and maximum (x_{max}) limits to E_{rad}/E_{Pen} (Han and Tian, 2018). This sigmoid generalized complementary function (SGCF) can be written as:

$$\frac{E}{E_{Pen}} = \frac{1}{1 + m\left(\frac{x_{max} - E_{rad}/E_{Pen}}{E_{rad}/E_{Pen} - x_{min}}\right)^{n}} \tag{3}$$

where x_{max} and x_{min} are the maximum and minimum values of E_{rad}/E_{Pen}, and m and n are parameters. The SGCF exhibits a three-stage pattern, and E/E_{Pen} increases approximately linearly with E_{rad}/E_{Pen} during the middle stage in environments that are neither too dry nor too wet. By making a first-order Taylor expansion of the SGCF at $E/E_{Pen} = 0.5$ equal to the linear AA function, parameters m and n can be transferred from α_e and b^{-1}:

$$\begin{cases} n = \frac{4\alpha_e(1+b^{-1})(x_{0.5} - x_{min})(x_{max} - x_{0.5})}{(x_{max} - x_{min})} \\ m = \left(\frac{x_{0.5} - x_{min}}{x_{max} - x_{0.5}}\right)^{n} \end{cases} \tag{4}$$

where $x_{0.5} = (0.5 + b^{-1})/(\alpha_e * (1 + b^{-1}))$ is the value of E_{rad}/E_{Pen} corresponding to $E/E_{Pen} = 0.5$. The linear AA function can be regarded as a special case of the SGCF (Han and Tian, 2018), for which $x_{min} = 0$ and $x_{max} = 1$ have been suggested for a daily scale because the function and simulated results are not sensitive to x_{min} and x_{max}. However, appropriate values for x_{min} and x_{max} at annual or multi-year timescales remain unclear.

Inspired by Han et al. (2012), Brutsaert (2015) generalized the CR to a fourth-order polynomial function between E/E_{Pen} and E_{po}/E_{Pen}, the application of which still requires specifying the methods of E_{Pen} and E_{po}. Considering the relationship with AA approach, this new polynomial function is regarded as the generalized nonlinear advection–aridity model (GNAA) and has the same variables as the AA function and SGCF; that is:

$$\frac{E}{E_{Pen}} = (2-c)\alpha_e^{2}\left(\frac{E_{rad}}{E_{Pen}}\right)^{2} - (1-2c)\alpha_e^{3}\left(\frac{E_{rad}}{E_{Pen}}\right)^{3} - c\alpha_e^{4}\left(\frac{E_{rad}}{E_{Pen}}\right)^{4} \tag{5}$$

where c is thought to be zero under usual situations (Brutsaert, 2015). Thus, a fixed $c = 0$ and calibrated parameter α_e of the GNAA have been adopted for daily (Ai et al., 2017; Brutsaert et al., 2017; Hu et al., 2018; Zhang et al., 2017), annual, and multi-year scales (Liu et al., 2016). However, the calibrated α_e was found to be less than unity with a fixed $c = 0$ in the Kahohu site in Japan (Ai et al., 2017), as well as for some eastern monsoon regions of China (Liu et al., 2016) that were thought to be unreasonable (Han and Tian, 2018). Thus, how α_e and c should be parameterized also remains unclear.

The GNAA and SGCF have both been applied to estimate evaporation at several locations (Brutsaert et al., 2017, 2020; Han and Tian, 2018; Zhang et al., 2017). Although they were compared at a daily scale by using data from flux towers (Han and Tian, 2018), setting their parameters for an annual timescale remains a major obstacle in their application. Thus, the main objective of this study was to evaluate the

Table 1
Basic characteristics of the 15 catchments.

Catchment	ID	Data length (years)	Area (km^2)	E_{Pen} (mm)	E_{rad} (mm)	P (mm)	R^a
Beiluo	C1	46	25,645	1076.0	734.6	528.2	0.73**
Fen	C2	47	38,728	1121.6	741.3	485.7	0.7**
Gushanchuan	C3	45	1263	1128.2	720.1	410.4	0.53**
Huangfu	C4	51	3175	1124.7	709.7	388.9	0.52**
Jing	C5	52	43,216	1060.2	730.2	505.8	0.73**
Kushui	C6	40	5216	1222.1	745.5	286.8	0.77**
Kuye	C7	52	8515	1166.7	716.5	386.8	0.63**
Qingjian	C8	50	3468	1124.3	734.0	474.0	0.75**
Qingshui	C9	40	14,489	1154.9	730.0	353.5	0.69**
Qiushui	C10	43	1873	1136.8	724.4	461.8	0.69**
Sanchuan	C11	40	4102	1125.4	732.7	470.0	0.77**
Tuwei	C12	50	3253	1169.9	724.4	392.3	0.65**
Wuding	C13	50	29,662	1171.3	728.1	395.6	0.78**
Xinshui	C14	50	3992	1122.7	745.2	504.6	0.68**
Yan	C15	50	5891	1074.3	727.1	484.4	0.72**
Mean	–	–	–	1131.9	729.6	435.3	0.69**

a. R is the correlation coefficient between E/E_{Pen} and E_{rad}/E_{Pen}.
** denotes $p < 0.01$.

GNAA and SGCF for estimating annual E for 15 catchments in the Loess Plateau, China, with water-balance-derived E and a focus on how parameters α_e, and/or c should be adopted for the GNAA, as well as how x_{min} and x_{max} should be adopted for the SGCF.

2. Materials and methods

2.1. Study area and data

The Loess Plateau is located in the upper and middle reaches of the Yellow River, China. As a typical non-humid region, the annual precipitation (P) is 200–750 mm, increasing from the northwest to the southeast (Tang et al., 2018). The climate is continental monsoon, with precipitation mainly concentrated between June and September, that experiences frequent rainstorms. The sparse vegetation resulted in severe soil erosion for a long period. The land use and land cover has been greatly changed because of the 'Grain for Green Project' implemented by the Chinese government in the Loess Plateau since 1999, which has contributed to the global greening trend (Chen et al., 2019). In this study, 15 typical catchments with areas ranging from 1263 to 43,216 km^2 were selected (Fig. 1 and Table 1). Monthly discharge data from 1960 to 2011 for all 15 catchments were provided by the Yellow River Conservancy Commission. Daily meteorological data for the period from 1960 to 2011 at 123 stations in and near the study area were obtained from the China Meteorological Administration and consist of air temperature, wind speed, and relative humidity data. Daily E_{Pen}, E_{rad} and P were calculated for each site, then were summed to obtain monthly values and spatially interpolated to obtain monthly averages on a catchment-scale by using the Kriging interpolation algorithm. Finally, monthly averages of E_{Pen}, E_{rad} and P were summed to obtain annual values.

2.2. Methods

Actual evaporation in the 15 catchments was calculated using the annual water balance equation, based on the water year, which aims at minimizing the water storage change in the catchments (Berghuijs and Woods, 2016; Carmona et al., 2014; Ning et al., 2017; Scott and Biederman, 2019; Sivapalan et al., 2011).

$$E_{obs} = P - R - \Delta S \tag{6}$$

In Eq. (6), P, R, and ΔS are annual precipitation, runoff, and the water storage change in a catchment, respectively. Water-balance-derived E was regarded as the 'observed' actual evaporation (E_{obs}). P was spatially averaged for each catchment from 123 meteorological sites, R was obtained from the outlet stations in the 15 catchments and the change in water storage was negligible in a water year.

The water year is defined by the American Meteorological Society (AMS; http://glossary.ametsoc.org/wiki/Water_year) as being from the beginning of the rainy season (soil moisture recharge) until the end of the season of maximum soil moisture utilization. However, the maximum evapotranspiration season is also in the rainy season because of rain and heat over the same period in the Loess Plateau, so the hydrological year ends with the end of the dry season which follows the rainy season. Thus, a period from May to the following April is defined as a water year on the Loess Plateau since the starting month for rainy season is May.

In this study, parameters of the generalized complementary functions were optimized by minimizing the mean absolute error (MAE) of the modeled and water-balance-derived E using the meteorological and hydrological data from 1960 to 2011. The GNAA was evaluated using three schemes: calibrating α_e with a fixed $c = 0$, calibrating c with a fixed $\alpha_e = 1.26$, and calibrating both c and α_e. Three parameter-calibrated schemes were also adopted for the SGCF: calibrating m and n with $x_{min} = 0$ and $x_{max} = 1$; calibrating m, n, and x_{max} with $x_{min} = 0$; and calibrating all four parameters (m, n, x_{min}, x_{max}). Evaporation estimation performances were evaluated by their determination coefficients (R^2), MAE, root mean square error (RMSE), and Nash-Sutcliffe efficiency coefficient (NSE) between the modeled E and the observed E. The algorithms of R^2, MAE, RMSE, and NSE are:

$$R^2 = \left(\frac{\sum_{i=1}^{n}(E_{mol,i} - \bar{E}_{mol})(E_{obs,i} - \bar{E}_{obs})}{\sqrt{\sum_{i=1}^{n}(E_{mol,i} - \bar{E}_{mol})^2 \cdot \sum_{i=1}^{n}(E_{obs,i} - \bar{E}_{obs})^2}}\right)^2 \tag{7}$$

$$MAE = \frac{\sum_{i=1}^{n}|E_{mol,i} - E_{obs,i}|}{n} \tag{8}$$

$$RMSE = \sqrt{\frac{\sum_{i=1}^{n}(E_{mol,i} - E_{obs,i})^2}{n}} \tag{9}$$

$$NSE = 1 - \frac{\sum_{i=1}^{n}(E_{mol,i} - E_{obs,i})^2}{\sum_{i=1}^{n}(E_{obs,i} - \bar{E}_{obs})^2} \tag{10}$$

where i and n denote the time series and length of the time sequence, respectively, and $E_{mol,i}$ and $E_{obs,i}$ are modeled values and observed values, respectively.

3. Results

3.1. Relationship between annual E_{rad}/E_{Pen} and E/E_{Pen}

For all 15 catchments, the annual E_{rad}/E_{Pen} and E/E_{Pen} are within a narrow range of [0.55, 0.73] and a broad range of [0.02, 0.73], respectively. Significant linear relationships between E/E_{Pen} and E_{rad}/E_{Pen} exist for all catchments; correlation coefficients range from 0.52 to 0.77, with a mean value of 0.69 (Table 1). The results from four example catchments located in the south (C1), east (C2), west (C6), and northern (C12) regions of the Loess Plateau are shown in Fig. 2. The linear relationship also exists for all catchments on the interannual scale (Fig. 3).

3.2. Effects of different parameterization methods in the GNAA

For the annual data from all catchments, by setting $c = 0$, the optimized α_e of the GNAA was 0.74 (Table 2) and the corresponding complementary curve of the GNAA does not fit the observed values well (Fig. 3). Most points are located below the GNAA curve with $\alpha_e = 1$ and $c = 0$, implying that the calibrated α_e would be less than unity if $c = 0$. If α_e is set to 1.26, the optimized c of the GNAA is 17.05 and the fitting

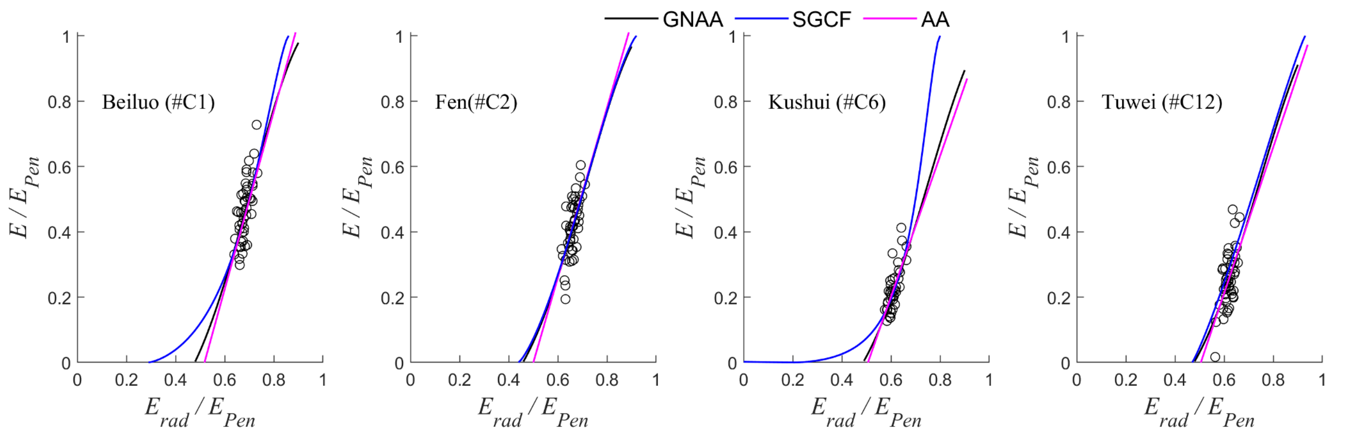

Fig. 2. Plots of annual E/E_{Pen} with respect to E_{rad}/E_{Pen} for four selected catchments, calculated according to the generalized nonlinear advection-aridity function (GNAA), sigmoid generalized complementary function (SGCF), and advection-aridity (AA) function.

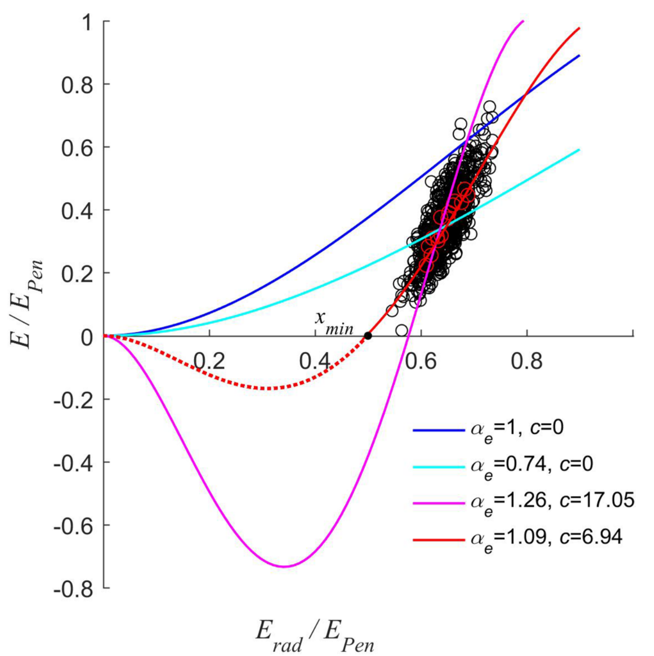

Fig. 3. Plots of annual E/E_{Pen} with respect to E_{rad}/E_{Pen} for all 15 catchments in the Loess Plateau compared with the GNAA for different parameterization schemes.

Table 2
Calibrated parameters and performances of the generalized nonlinear advection-aridity function (GNAA) and the sigmoid generalized complementary function (SGCF) using three parameter-constrained schemes.

	GNAA				SGCF					
	α_e	c	R^2	MAE	α_e	$1/b$	x_{min}	x_{max}	R^2	MAE
Case 1	0.74	0	0.21	78.4	1.17	1.77	0	1	0.51	59.3
Case 2	1.26	17.05	0.55	107.1	1.17	1.78	0	0.96	0.51	59.3
Case 3	1.09	6.94	0.52	58.9	1.14	1.47	0.51	0.87	0.52	58.8
AA*					1.13	1.39	0.52	0.88	0.52	58.8

Note: the advection-aridity (AA) function is regarded as a special case of the SGCF where $x_{min} = 1/[\alpha_e(1 + b)]$ and $x_{max} = 1/\alpha_e$.

degree of the GNAA curve to the observed data increases significantly. However, the simulated E/E_{Pen} would be less than zero if $E_{rad}/E_{Pen} < 0.58$. The fitting degree of the GNAA curve to the observed data would further increase if both α_e and c were calibrated (1.09 and 6.94, respectively) and the curve was above y = 0 if $E_{rad}/E_{Pen} > 0.49$ (x_{min} in Fig. 3). The curve within the range of the observed data approaches a straight line.

3.3. Effects of different parameterization methods in the SGCF

For fixed $x_{min} = 0$ and $x_{max} = 1$, the SGCF with calibrated m and n values fits the observed data well (Fig. 4). The calibrated α_e was 1.17, which is located in a reasonable range of the Priestley-Taylor coefficient. The curve shows little change if x_{max} is added for calibration (the calibrated value of x_{max} is 0.96). However, the two curves of the SGCF with $x_{min} = 0$ depart from the lower parts of the scatter plots. The fit of the SGCF curve is improved if x_{min} is also added for calibration (Table 2). Calibrated x_{min} and x_{max} values were 0.51 and 0.87, respectively, which are outside their recommended ranges at a daily timescale. Similar results were found for the four selected catchments (Fig. 2). The SGCF curve with four calibrated parameters was nearly equal to the linear AA curves for all 15 catchments.

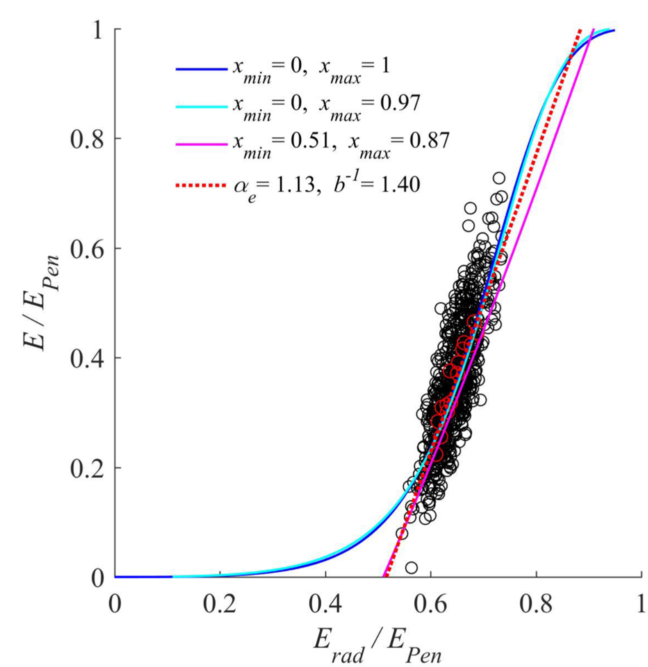

Fig. 4. Plots of annual E/E_{Pen} with respect to E_{rad}/E_{Pen} for all 15 catchments in the Loess Plateau compared with the SGCF using different parameterization schemes. The red dotted line represents the theoretical line of the AA function.

Table 3
Performances of the GNAA, SGCF, and AA functions for 15 catchments in the Loess Plateau.

		GNAA					SGCF					AA				
ID	E_{obs}	R^2	MAE	RMSE	NSE	E_{mol}	R^2	MAE	RMSE	NSE	E_{mol}	R^2	MAE	RMSE	NSE	E_{mol}
C1	496.5	0.24	56.0	69.3	0.23	494.1	0.25	55.9	68.7	0.24	490.2	0.24	56.0	69.4	0.23	487.8
C2	462.6	0.29	53.1	70.4	0.28	458.5	0.29	53.1	70.4	0.28	465.8	0.29	53.1	70.2	0.29	465.5
C3	355.9	0.08	58.1	73.0	0.06	362.8	0.12	57.6	73.9	0.04	355.3	0.12	57.6	73.8	0.04	355.3
C4	350.4	0.06	54.6	67.9	0.06	344.4	0.07	55.0	68.1	0.05	343.5	0.08	54.3	67.4	0.07	347.4
C5	468.9	0.29	48.2	64.1	0.27	467.6	0.28	48.1	63.9	0.27	469	0.29	48.2	64.1	0.26	467.3
C6	270.5	0.48	38.8	51.4	0.47	259.9	0.47	38.3	51.4	0.47	266	0.47	39.0	51.6	0.46	265.1
C7	328.0	0.24	49.1	62.9	0.23	325.0	0.24	49.0	62.7	0.24	326	0.25	48.8	62.4	0.24	324.8
C8	435.2	0.36	57.3	70.5	0.35	421.5	0.36	57.2	70.8	0.35	426	0.36	57.4	70.4	0.35	428.0
C9	346.0	0.31	43.6	58.6	0.29	335.5	0.31	43.5	58.5	0.29	334.7	0.32	43.4	58.4	0.29	334.8
C10	423.4	0.34	66.8	82.9	0.31	403.8	0.34	66.6	82.6	0.32	407.6	0.34	66.8	83.1	0.31	406.4
C11	413.5	0.47	55.7	70.1	0.43	416.0	0.46	55.5	69.4	0.44	405.8	0.47	55.7	70.1	0.43	406.4
C12	295.6	0.28	56.1	73.1	0.28	292.0	0.28	56.3	73.5	0.27	294.6	0.29	55.9	72.7	0.29	294.4
C13	359.3	0.43	41.2	54.5	0.43	358.9	0.45	41.0	54.0	0.44	362	0.42	41.3	55.0	0.42	363.7
C14	476.3	0.28	60.8	78.0	0.27	491.0	0.28	60.7	78.0	0.27	475.3	0.28	60.9	78.0	0.27	482.1
C15	451.0	0.3	55.5	70.6	0.27	429.8	0.29	55.5	70.5	0.28	440.7	0.30	55.5	70.6	0.27	438.6
Mean	395.5	0.3	53.0	67.8	0.28	390.7	0.30	52.9	67.8	0.28	390.8	0.30	52.3	67.8	0.28	391.2

3.4. Annual evaporation estimation performances of GNAA and SGCF

The performances of GNAA and SGCF, as well as the AA model, were compared for modeling annual E for the 15 catchments of the Loess Plateau (Table 3), and their optimized parameters are shown in Table 4. Generally, the discrepancies among the three complementary functions for actual evaporation estimation are small. The SGCF performed better than the GNAA and AA functions for most of the catchments. The relative errors of the simulated E and water-balance-derived E were 0.11–4.7%, 0.02–3.7%, and 0.02–3.73% for the GNAA, SGCF, and AA models in the 15 catchments, respectively. The two catchments (C3, C4) in the northern region were characterized by much smaller R^2 and NSE values than the other catchments, which might reflect their smaller areas and the fact that they contained no meteorological sites.

The ranges of parameters α_e and c of the GNAA were [0.91, 1.18] and [2.73, 11.18], respectively; the ranges of parameter α_e and b^{-1} for the AA model were [0.89, 1.24] and [0.58, 2.25], respectively. For the SGCF, the range of parameter α_e was [1.03,1.27] with an average value of 1.15; the ranges of parameter b^{-1}, x_{min} and x_{max} were [1.05, 2.78], [0.16, 0.54] and [0.78, 0.98], respectively. In catchments C6, C10, C11, and C13, the optimized α_e of SGCF was approximately 1.26 (Table 4).

4. Discussion

4.1. Priestley-Taylor coefficient in generalized complementary functions

The Priestley-Taylor coefficient α_e is the common parameter in complementary functions and has been thought to range from 1.0 to 1.5 (Brutsaert and Chen, 1995). It was reported that calibrated values of α_e for the AA model were 1.18, 1.00, and 1.04 in Central Sweden, Eastern China, and Northwestern Cyprus, respectively (Xu and Singh, 2005), and that the average of parameter α_e for the AA model was 1.18 using the First International Field Experiment data (Szilagyi, 2007). In four different climate and land use types in Australia, α_e calibrated for the GNAA ranged from 1.04 to 1.19 (Zhang et al., 2017), while it ranged from 1.01 to 1.02 for three heights in the semi-humid regions of the Loess Plateau (Brutsaert et al., 2017), and from 0.98 to 1.1 for four sites with differing elevations on Gongga mountain, southwest of China (Hu et al., 2018). Mean values of $\alpha_e = 1.12$ and 1.13 were determined from observational data using the modified GNAA for the whole China (Ma et al., 2019) and for 334 basins in the United States (Szilagyi et al., 2017). Han and Tian (2018) obtained the ranges of α_e to [0.9, 1.29] for the GNAA and [0.97, 1.40] for the SGCF with constraining $x_{min} = 0$ and $x_{max} = 1$ at 20 flux stations in different representative biomes. For the Tibetan Plateau, China, the α_e calibrated for the SGCF is 1.02 (Ma et al.,

Table 4
Optimized parameters for the GNAA, SGCF, and AA functions.

		GNAA			SGCF				AA		
ID	$x_{min,\ obs}$	α_e	c	x_{min}	α_e	$1/b$	x_{min}	x_{max}	α_e	$1/b$	x_{min}
C1	0.64	1.09	6.45	0.48	1.15	1.55	0.29	0.86	1.13	1.41	0.52
C2	0.62	1.08	5.89	0.46	1.13	1.32	0.44	0.92	1.13	1.3	0.50
C3	0.56	0.96	3.52	0.32	1.05	1.05	0.49	0.98	1.05	1.07	0.49
C4	0.56	0.91	2.73	0.20	1.03	1.07	0.16	0.98	0.89	0.58	0.41
C5	0.64	1.10	7.99	0.53	1.08	1.17	0.47	0.93	1.15	1.70	0.55
C6	0.57	1.03	6.02	0.49	1.24	2.78	0.21	0.80	1.03	1.09	0.51
C7	0.55	1.06	5.66	0.45	1.08	1.16	0.46	0.96	1.04	1.01	0.48
C8	0.61	1.12	7.80	0.51	1.18	1.74	0.41	0.93	1.17	1.64	0.53
C9	0.59	1.04	5.70	0.47	1.08	1.23	0.47	0.97	1.06	1.16	0.51
C10	0.59	1.15	8.45	0.51	1.27	2.52	0.26	0.78	1.20	1.72	0.53
C11	0.62	1.18	11.18	0.55	1.24	2.36	0.54	0.79	1.24	2.25	0.56
C12	0.56	1.04	5.93	0.48	1.15	1.73	0.39	0.90	1.05	1.13	0.51
C13	0.58	1.11	6.91	0.49	1.25	2.23	0.33	0.82	1.14	1.34	0.50
C14	0.62	1.13	7.51	0.50	1.19	1.73	0.36	0.84	1.18	1.60	0.52
C15	0.64	1.09	7.61	0.52	1.15	1.62	0.48	0.91	1.15	1.63	0.54
Mean	0.60	1.07	6.62	0.46	1.15	1.68	0.38	0.89	1.11	1.38	0.51

Note: x_{min} of GNAA is equal to$[2c-1-(1+4c)^{1/2}]/(2c\alpha_e)$ (Liu et al., 2020); x_{min} in the AA model was calculated by the same manner as in Table 2.

2015a), while it became 1.13 for AA model (Ma et al., 2015b). In this study, the averages calibrated by the GNAA, SGCF, and AA with annual data from the Loess Plateau were 1.07, 1.15 and 1.11, respectively, which are approximately consistent with previous studies. The calibrated α_e from the SGCF was closest to the widely accepted value of 1.26.

Although it has been reported that the sensitivity of parameter α_e to E is greater than that of parameter c to E (Liu et al., 2016; Szilagyi et al., 2017), the relative variations in calibrated parameter α_e for the 15 catchments were less than those of c (*or* b^{-1}). The optimized α_e varies for the 15 catchments with a standard deviation (SD) of 0.07 and a coefficient of variation (C_v) of 0.06 for GNAA, which is much less than the values of c (with SD of 1.95 and C_v of 0.29, respectively). Similar results were also found for the SGCF and AA functions, in which the (SD, C_v) for α_e are (0.07, 0.06) and (0.08, 0.08), respectively, and those for b^{-1} are (0.54, 0.32) and (0.39, 0.28), respectively. The relatively stable α_e suggests that generalized complementary functions may be used with a constant α_e (Han et al., 2012).

GNAA is a nonlinear improvement based on the linear AA model and more boundary conditions. The linear AA function could be regarded as a special case of the SGCF, and the parameters of the SGCF were estimated with the aid of AA model because the complementary curves are approximately linear when E_{rad}/E_{Pen} is neither excessively large nor excessively small (Han and Tian, 2018). Therefore, there is an intrinsic connection among the three models. The three functions are approximately equivalent under conditions neither too dry nor too wet. Therefore, the calibrated α_e values from the three models are significantly correlated: with correlation coefficients of 0.72 between the GNAA and SGCF, 0.95 between the GNAA and AA, and 0.64 between the SGCF and AA. In this study, the performances of the GNAA, SGCF, and AA for estimating annual evaporation rates with fixed α_e (1.07, 1.15, and 1.11, respectively) from 15 catchments were also evaluated. Few differences in model performances were observed among the three models, with mean MAE increasing from 53.0, 52.9, and 52.3 to 54.3, 53.6, and 54.7 mm, respectively (Table 3 and 5). If α_e is set as a constant value, the burden of parameter calibration for generalized complementary functions is reduced, with acceptable performances weakening.

4.2. Lower limit of E_{rad}/E_{Pen}

The lower limit of E_{rad}/E_{Pen} is controversial in the use of complementary functions. Zero is generally regarded as the lower limit for E_{rad}/E_{Pen} in the GNAA and in the original version of the SGCF (Han et al., 2012). However, E_{rad}/E_{Pen} does not necessarily equal zero when $E/E_{Pen} = 0$, as it is almost impossible for E_{Pen} to reach infinity for a certain large E_{rad} (Crago et al., 2016; Crago and Qualls, 2018; Szilagyi et al., 2017). In the SGCF, the lower limit was modified to $E/E_{Pen} = 0$ at $E_{rad}/E_{Pen} = x_{min}$. At short timescales (daily or hourly), x_{min} may approach zero when the energy input is small; however, x_{min} would be much larger than zero at longer timescales as E_{rad} is much larger than zero (Han and Tian, 2018). The minimum values of observed annual E_{rad}/E_{Pen} ranged from 0.52 to 0.73 with a mean value of 0.64 for the 15 catchments in the Loess Plateau. The optimized x_{min} of the SGCF ranged from 0.16 to 0.54, with a mean value of 0.38. The inclusion of x_{min} improved the performance of the SGCF when estimating annual evaporation.

One of four boundary conditions in the GNAA requires that the start point of the curve is the origin, i.e., $E/E_{Pen} = 0$ at $E_{rad}/E_{Pen} = 0$. However, the curve has two intersection points on the horizontal axis if c is larger than 2 (Fig. 3). Thus, the second intersection point should be used as the starting point, which corresponds to the boundary condition of $E/E_{Pen} = 0$ at $E_{rad}/E_{Pen} = x_{min}$ (Liu et al., 2020). The x_{min} values of the GNAA for each catchment are shown in Table 4 and range from 0.2 to 0.55, with an average of 0.46.

4.3. Impact of spatial interpolation methods on parameters

Meteorological data from observation sites were used to calculate daily E_{rad} (or E_{Pen}) in this study, and then monthly E_{rad} (or E_{Pen}) and P were interpolated using the Kriging algorithm, which is called the "calculate-then-interpolate" method. However, some researchers spatially average the meteorological data first, then calculate daily and even annual E_{rad} (or E_{Pen}), which is called the "interpolate-then-calculate" method. However, the latter method accumulates the interpolation error of the input variables; in contrast, the former method only interpolates once and thus introduces smaller errors (Mardikis et al., 2005). In addition, different interpolation algorithms have little effect on the parameters. For example, the CoKriging interpolation method, based on the Kriging method with elevation as an additional input, was used to spatially average E_{Pen} (denoted $E_{Pen\text{-}CoK}$), E_{rad} (denoted $E_{rad\text{-}CoK}$), and P (denoted P_{CoK}). The MAE of E_{Pen}, E_{rad}, and P between those obtained by the Kriging and CoKriging interpolation algorithms were 8.9 mm/year, 3.7 mm/year, and 10.8 mm/year, respectively, for all 15 catchments (Table A.1), which are less than the uncertainties in parameter calibration obtained using the minimizing MAE (approximately 53 mm) between E_{obs} and E_{mol} (Table 3). Moreover, when $E_{Pen\text{-}Cok}$, $E_{rad\text{-}Cok}$, and P_{Cok} were used to calibrate the parameters of the GNAA, SGCF and AA (Table A.1), the mean α_e and c in the GNAA, α_e, $1/b$, x_{min} and x_{max} in the SCGF, and α_e and $1/b$ in the AA were (1.05, 5.95), (1.14,

Table 5
Optimized parameters and model performances with parameters restricted by fixed α_e.

	GNAA with a fixed value of $\alpha_e = 1.07$					SGCF with a fixed value of $\alpha_e = 1.15$							AA with a fixed value of $\alpha_e = 1.11$				
ID	c	R^2	MAE	RMSE	NSE	b^{-1}	x_{min}	x_{max}	R^2	MAE	RMSE	NSE	b^{-1}	R^2	MAE	RMSE	NSE
C1	5.68	0.22	56.3	69.8	0.22	1.53	0.18	0.93	0.25	55.9	68.7	0.24	1.31	0.52	59.0	74.1	0.51
C2	5.33	0.27	53.5	71.1	0.27	1.45	0.17	0.93	0.29	53.2	70.4	0.28	1.24	0.22	56.4	70.0	0.21
C3	6.44	0.12	59.7	76.8	−0.04	1.74	0.15	0.89	0.09	59.2	75.7	−0.01	1.19	0.27	53.5	70.9	0.27
C4	6.31	0.12	58.5	72.2	−0.07	1.72	0.07	0.88	0.09	57.1	70.6	−0.02	1.36	0.14	59.9	77.9	−0.07
C5	6.51	0.26	49.0	64.4	0.26	1.68	0.34	0.96	0.28	48.1	63.9	0.27	1.33	0.14	59.2	73.0	−0.09
C6	6.87	0.48	39.4	50.6	0.48	1.80	0.25	1	0.48	38.5	51.3	0.47	1.38	0.26	49.2	64.6	0.26
C7	5.91	0.24	49.3	63.0	0.23	1.54	0.43	0.87	0.24	49.4	63.2	0.22	1.40	0.48	40.8	50.9	0.48
C8	5.76	0.32	59.7	73.3	0.30	1.47	0.47	0.96	0.35	57.9	71.1	0.34	1.27	0.26	49.8	63.4	0.22
C9	6.49	0.32	43.8	57.4	0.31	1.66	0.45	0.88	0.32	44.0	57.6	0.31	1.25	0.32	59.6	73.0	0.31
C10	5.27	0.28	67.7	86.4	0.25	1.38	0.47	0.97	0.31	67.1	84.0	0.29	1.35	0.33	44.0	57.1	0.32
C11	5.92	0.41	61.1	73.5	0.38	1.51	0.51	0.98	0.44	58.3	70.2	0.43	1.17	0.29	67.7	85.7	0.26
C12	6.71	0.29	56.3	72.6	0.29	1.75	0.41	0.87	0.28	56.3	73.5	0.27	1.28	0.41	60.7	72.9	0.38
C13	5.62	0.41	41.4	56.2	0.39	1.47	0.28	0.95	0.41	41.3	56.1	0.40	1.37	0.30	56.5	72.4	0.30
C14	5.55	0.25	62.8	79.9	0.24	1.45	0.39	0.95	0.27	61.7	78.4	0.27	1.22	0.41	41.3	55.5	0.41
C15	6.42	0.27	56.4	71.3	0.26	1.67	0.24	0.95	0.29	55.6	70.5	0.27	1.22	0.26	62.7	79.8	0.24
Mean	6.05	0.28	54.3	69.2	0.25	1.59	0.32	0.93	0.29	53.6	68.3	0.27	1.29	0.31	54.7	69.4	0.25

1.61, 0.21, 0.94) and (1.07, 1.23) for all catchments, respectively, which were similar to the values in Table 4. Only in a few catchments, such as the Gushanchuan, Kushui and Sanchuan, there were obvious parameter differences. Furthermore, additional high-precision grid meteorological data are now available, which would benefit accurate calculation of E_{rad} (or E_{Pen}, P, etc.) and parameter estimations at a catchment scale.

5. Conclusions

Two generalized complementary functions, the GNAA and the SGCF, were validated and compared with annual water-balance-derived data from 15 catchments in the Loess Plateau, China. For the GNAA at an annual timescale, it is necessary to optimize parameters α_e and c to accurately estimate annual E. For the SGCF at an annual scale, the upper and lower limits of the SGCF need to be constrained when estimating E. After calibration, the SGCF performs a little better than the GNAA, and the calibrated α_e from the SGCF is closer to 1.26 than that of the GNAA. As relative variations in α_e are much smaller than in other parameters, the generalized complementary functions have the potential to be applied with α_e set as a constant value with little weakening of the model performance. This allows for a reduced burden of parameter calibration.

CRediT authorship contribution statement

Haixiang Zhou: Conceptualization, Formal analysis, Writing - original draft. **Songjun Han:** Software, Validation, Writing - review & editing. **Wenzhao Liu:** Supervision, Conceptualization, Writing - review & editing.

Declaration of Competing Interest

The authors declare that they have no known competing financial interests or personal relationships that could have appeared to influence the work reported in this paper.

Acknowledgements

This study was supported by the National Natural Science Foundation of China [grant numbers 41971049, 41571036] and by the National Key Research and Development Program of China [grant number 2016YFC0501602].

Appendix

Table A.1
E_{Pen}, E_{rad} and P variables interpolated using the CoKriging method and its corresponding optimized parameters for the GNAA, SGCF, and AA models.

					GNAA		SGCF				AA	
ID	E_{Pen_CoK}	E_{rad_CoK}	P_{CoK}	$x_{min,\ obs}$	α_e	c	α_e	$1/b$	x_{min}	x_{max}	α_e	$1/b$
C1	1070.31	731.95	529.3	0.64	1.09	6.47	1.15	1.48	0.2	0.95	1.14	1.41
C2	1122.96	742.27	486.29	0.61	1.1	6.58	1.16	1.55	0.15	0.93	1.14	1.42
C3	1125.15	723.91	414.09	0.56	0.82	1.39	1.02	1.08	0.1	0.99	0.78	0.37
C4	1117.67	712.54	393.74	0.57	0.93	2.87	1.01	0.95	0.32	1	0.95	0.71
C5	1062.02	729.73	503.49	0.64	1.09	7.6	1.16	1.76	0.22	0.95	1.14	1.62
C6	1233.46	744.59	282.61	0.56	1.01	5.56	1.13	1.74	0.26	0.96	0.99	0.98
C7	1166.76	717.42	384.51	0.54	1.06	5.77	1.1	1.29	0.45	0.95	1.06	1.06
C8	1123.97	736.06	476.82	0.62	1.13	7.85	1.19	1.84	0.12	0.91	1.18	1.67
C9	1162.79	729.27	344.38	0.58	1.04	5.86	1.23	2.39	0.11	0.84	1.04	1.07
C10	1142.12	721.65	459.86	0.58	1.03	4.08	1.09	1.12	0.12	0.95	1.05	0.92
C11	1131.13	731.08	468.33	0.6	1.11	7.47	1.15	1.48	0.49	0.96	1.15	1.49
C12	1173.33	727.24	390.82	0.56	1.05	6.24	1.12	1.59	0.26	0.95	1.05	1.15
C13	1176	728.89	393.63	0.58	1.1	6.6	1.2	1.83	0.14	0.9	1.14	1.35
C14	1116.32	741.72	506.48	0.63	1.13	7.97	1.22	2.08	0.14	0.89	1.18	1.69
C15	1063.28	727.04	489.46	0.64	1.07	6.98	1.17	1.92	0.14	0.89	1.13	1.58
Mean	1132.48	729.69	434.92	0.59	1.05	5.95	1.14	1.61	0.21	0.93	1.07	1.23

Note: $E_{Pen\text{-}Cok}$, $E_{rad\text{-}Cok}$ and P_{Cok} denote the spatially-averaged apparent potential evaporation, radiation term and Precipitation by using the CoKriging algorithm for each catchment.

References

Ai, Z., Wang, Q., Yang, Y., Manevski, K., Zhao, X., Ear, D., 2017. Estimation of land-surface evaporation at four forest sites across Japan with the new nonlinear complementary method. Sci. Rep. 7, 17793.

Berghuijs, W.R., Woods, R.A., 2016. Correspondence: space-time asymmetry undermines water yield assessment. Nat. Comm. 7, 11603.

Brutsaert, W., 2015. A generalized complementary principle with physical constraints for land-surface evaporation. Water Resour. Res. 51 (10), 8087–8093.

Brutsaert, W., Chen, D.Y., 1995. Desorption and the 2 stages of drying of natural tallgrass prairie. Water Resour. Res. 31 (5), 1305–1313.

Brutsaert, W., Cheng, L., Zhang, L., 2020. Spatial distribution of global landscape evaporation in the early twenty first century by means of a generalized complementary approach. J. Hydrometeorol.

Brutsaert, W., Li, W., Takahashi, A., Hiyama, T., Zhang, L., Liu, W., 2017. Nonlinear advection-aridity method for landscape evaporation and its application during the growing season in the southern Loess Plateau of the Yellow River basin. Water Resour. Res. 53 (1), 270–282.

Brutsaert, W., Parlange, M.B., 1998. Hydrologic cycle explains the evaporation paradox. Nature 396 (6706), 30–30.

Brutsaert, W., Stricker, H., 1979. An advection-aridity approach to estimate actual regional evapotranspiration. Water Resour. Res. 15 (2), 443–450.

Carmona, A.M., Sivapalan, M., Yaeger, M.A., Poveda, G., 2014. Regional patterns of interannual variability of catchment water balances across the continental U.S.: a Budyko framework. Water Resour. Res. 50 (12), 9177–9193.

Chen, C., Park, T., Wang, X., Piao, S., Xu, B., Chaturvedi, R.K., Fuchs, R., Brovkin, V., Ciais, P., Fensholt, R., Tommervik, H., Bala, G., Zhu, Z., Nemani, R.R., Myneni, R.B., 2019. China and India lead in greening of the world through land-use management. Nat. Sustain. 2, 122–129.

Crago, R., Szilagyi, J., Qualls, R., Huntington, J., 2016. Rescaling the complementary relationship for land surface evaporation. Water Resour. Res. 52 (11), 8461–8471.

Crago, R.D., Qualls, R.J., 2018. Evaluation of the generalized and rescaled complementary evaporation relationships. Water Resour. Res. 54 (10), 8086–8102.

Granger, R.J., 1989. A complementary relationship approach for evaporation from nonsaturated surfaces. J. Hydrol. 111 (1–4), 31–38.

Granger, R.J., Gray, D., 1989. Evaporation from natural nonsaturated surfaces. J. Hydrol. 111 (1), 21–29.

Han, S., Hu, H., Yang, D., Tian, F., 2011. A complementary relationship evaporation model referring to the Granger model and the advection-aridity model. Hydrol. Process. 25 (13), 2094–2101.

Han, S., Tian, F., 2018. Derivation of a sigmoid generalized complementary function for

evaporation with physical constraints. Water Resour. Res. 54 (7), 5050–5068.
Han, S.J., Hu, H.P., Tian, F.Q., 2012. A nonlinear function approach for the normalized complementary relationship evaporation model. Hydrol. Process. 26 (26), 3973–3981.
Han, S.J., Hu, H., Tian, F., 2008. Evaluating the advection-aridity model of evaporation using data from field-sized surfaces of HEIFE. International Symposium on Flood Forecasting & Water Resources Assessment for Iahs-pub.
Hu, Z., Wang, G., Sun, X., Zhu, M., Song, C., Huang, K., Chen, X., 2018. Spatial-temporal patterns of evapotranspiration along an elevation gradient on Mount Gongga, Southwest China. Water Resour. Res. 54 (6), 4180–4192.
Liu, X., Liu, C., Brutsaert, W., 2016. Regional evaporation estimates in the eastern monsoon region of China: assessment of a nonlinear formulation of the complementary principle. Water Resour. Res. 52 (12), 9511–9521.
Liu, W., Zhou, H., Han, X., Li, Z., 2020. Comment on two papers about the generalized complementary evaporation relationships by Crago et al. Water Resour. Res. 56 (3), e2019WR026292.
Ma, N., Szilagyi, J., Zhang, Y., Liu, W., 2019. Complementary-relationship-based modeling of terrestrial evapotranspiration across China during 1982–2012: validations and spatiotemporal analyses. J. Geophys. Res. Atmos. 124 (8), 4326–4351.
Ma, N., Zhang, Y., Szilagyi, J., Guo, Y., Zhai, J., Gao, H., 2015b. Evaluating the complementary relationship of evapotranspiration in the alpine steppe of the Tibetan Plateau. Water Resour. Res. 51 (2), 1069–1083.
Ma, N., Zhang, Y., Xu, C.Y., Szilagyi, J., 2015a. Modeling actual evapotranspiration with routine meteorological variables in the data-scarce region of the Tibetan Plateau: comparisons and implications. J. Geophys. Res. Biogeosci. 120 (8), 1638–1657.
Mardikis, M.G., Kalivas, D.P., Kollias, V.J., 2005. Comparison of interpolation methods for the prediction of reference evapotranspiration - an application in Greece. Water Resour. Manag. 19 (3), 251–278.
Morton, F.I., 1978. Estimating evapotranspiration from potential evaporation: practicality of an iconoclastic approach. J. Hydrol. 38 (1), 1–32.
Morton, F.I., 1983. Operational estimates of areal evapotranspiration and their significance to the science and practice of hydrology. J. Hydrol. 66 (1), 1–76.
Ning, T., Li, Z., Liu, W., 2017. Vegetation dynamics and climate seasonality jointly control the interannual catchment water balance in the Loess Plateau under the Budyko framework. Hydrol. Earth Syst. Sci. 21 (3), 1515.
Penman, H.L., 1948. Natural evaporation from open water, bare soil and grass. Proc. R. Soc. A. 193, 120–146.
Priestley, C.H.B., Taylor, R.J., 1972. On the assessment of surface heat flux and evaporation using large-scale parameters. Month. Weather Rev. 100 (2), 81–92.
Scott, R.L., Biederman, J.A., 2019. Critical zone water balance over 13 years in a Semiarid Savanna. Water Resour. Res. 55 (1), 574–588.
Sivapalan, M., Yaeger, M.A., Harman, C.J., Xu, X., Troch, P.A., 2011. Functional model of water balance variability at the catchment scale: 1. Evidence of hydrologic similarity and space-time symmetry. Water Resour. Res. 47 (2), 2144–2150.
Szilagyi, J., 2007. On the inherent asymmetric nature of the complementary relationship of evaporation. Geophys. Res. Lett. 340 (2), 155–164.
Szilagyi, J., Crago, R., Qualls, R., 2017. A calibration-free formulation of the complementary relationship of evaporation for continental-scale hydrology. J. Geophys. Res. Atmos. 122 (1), 264–278.
Tang, X., Miao, C., Xi, Y., Duan, Q., Lei, X., Li, H., 2018. Analysis of precipitation characteristics on the loess plateau between 1965 and 2014, based on high-density gauge observations. Atmos. Res. 213, 264–274.
Xu, C.Y., Singh, V.P., 2005. Evaluation of three complementary relationship evapotranspiration models by water balance approach to estimate actual regional evapotranspiration in different climatic regions. J. Hydrol. 308 (1–4), 105–121.
Zhang, L., Cheng, L., Brutsaert, W., 2017. Estimation of land surface evaporation using a generalized nonlinear complementary relationship. J. Geophys. Res. Atmos. 122 (3), 1475–1487.